

# The determination and enhancement of compliant modes for actuation in structural assemblies

James Bird<sup>a,\*</sup>, Matthew Santer<sup>a</sup>, Jonathan Morrison<sup>a</sup>

<sup>a</sup>*Department of Aeronautics, Imperial College London  
Prince Consort Road, London. SW7 2AZ, UK*

---

## Abstract

Linear algebra methods for determining modes of kinematic and static indeterminacy in jointed frames are extended to reveal modes of compliance in otherwise rigid assemblies. These modes are extracted from a structural model, based on finite elements, via a singular value decomposition and yield the ways in which a structure can be most easily deformed. This modal approach also allows for the formulation of a reduced-order structural model, whereby relevant modes are selected and used as the basis for the optimisation of a compliant structure. The method detailed is shown to be a useful design tool, demonstrated by its application to a structure based on the Kagome lattice geometry. For certain frameworks, first order effects produce tightening under actuation. As a result, a scheme to adjust the modes to take nonlinear effects into account is also given.

*Keywords:* Adaptive structures, Kagome lattice, SVD

*2010 MSC:* 00-01, 99-00

---

---

\*Corresponding author

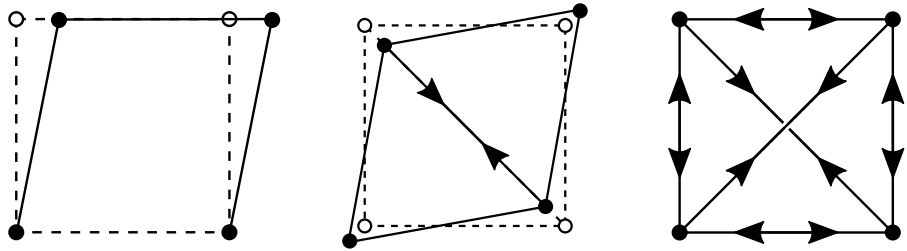
*Email address:* [j.bird12@imperial.ac.uk](mailto:j.bird12@imperial.ac.uk) (James Bird)

## 1. Introduction

Compliant mechanisms offer elegant engineering solutions to problems that are typically tackled with conventional components. In a compliant mechanism the modes of displacement produced by joints, bearings and sliders can be replicated by allowing modes of compliance in an otherwise rigid assembly [1]. This approach has wide ranging applications, from deployable space structures [2] to morphing aircraft wings [3] as well as everyday household products [1].

By having no complex moving parts, compliant structures are generally easier to maintain and manufacture than the mechanisms which they emulate. They offer a solution when manufacturing small sizes or large quantities of joints is impractical or the cost prohibitive. A systematic method for the determination of modes of deformation in compliant structures is currently lacking. In this paper, we take linear algebra methods which have traditionally been used to analyse pin-jointed frames for determinacy, and adapt them to find orthogonal modes of compliance in rigid-jointed frameworks. In this way, structures can be designed such that modes of deformation correspond with desired paths of actuation, while regions that are required to have structural stiffness are bolstered. This is akin to a pin-jointed structure, with a single mode of kinematic indeterminacy corresponding to a desired inextensible mechanism.

In this paper we take existing methods used for analysing pin-jointed frames, and extend them to continuous assemblies. A general method for determining modes of compliance from a finite element discretisation is presented, and examples are provided using beam elements. A scheme to account for geometrically nonlinear effects is also detailed. Finally, using these tools, the design of a compliant structure based on the Kagome lattice geometry is presented. The process illustrates how a structure with many degrees of freedom can be reduced to a small number of key modes, which are then used as the basis of an efficient optimisation routine for the design of adaptive compliant structures.



(a) A structure with a mode of kinematic indeterminacy.      (b) A structure which is both kinematically and statically determinate.      (c) A structure which is statically indeterminate.

Figure 1: Three pin-jointed structures showing how different configurations of members can produce structures which are determinate, mechanisms or capable of sustaining self-stress.

## 2. Evaluation of compliant modes using the SVD

30 In this section, the construction of a quasi-stiffness matrix  $\beta$  for a continuous structure is detailed. This matrix is then factorised using a singular value decomposition (SVD), and physically relevant modes of compliance are extracted. Algebraic analysis of pin-jointed frames to determine their structural characteristics is well established, and forms the basis of our method. We begin with a  
 35 recap of this approach.

### 2.1. Pin-jointed frame analysis

Maxwell [4] showed that a three dimensional frame can be considered ‘simply stiff’, with no redundant elements or mechanisms, if the number of elements  $m$  is related to the number of frictionless joints  $j$  by

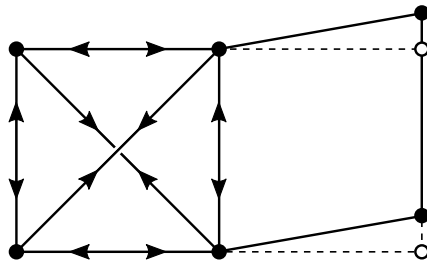
$$m = 3j - 6 \tag{1}$$

40 If the frame is two dimensional, the relation becomes

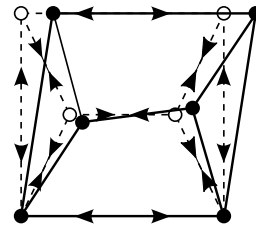
$$m = 2j - 3 \tag{2}$$

Maxwell's rule originates from the idea that in order for the stress-state of the structure to be unique, the number of equations relating the elongations of the members to the displacements at the nodes has to match the number of degrees of freedom of the system.

45 This principle is demonstrated in Figure 1, illustrating how the determinacy of a four noded structure can be altered with different connections. Figure 1a shows a pin-jointed structure with modes of kinematic indeterminacy. In this case, the number of compatibility equations is less than the number of degrees of freedom, and hence nodes are able to move freely, observed as an inextensional mechanism. In Figure 1b, Maxwell's rule in equation 2 is satisfied, and the structure is 'simply stiff'. The nodal displacements can be equated uniquely to the elongation of the bars, and similarly, any extension of members does



(a) A framework which obeys Maxwell's rule yet has both regions of self stress, and a finite inextensional mechanism



(b) A structure possessing a mode of static and kinematic indeterminacy. These modes then interact to cause the inextensible mechanism to tighten with displacement, resulting in an infinitesimal mechanism

Figure 2: Two configurations of pin-jointed frames which obey Maxwell's rule, but behave unexpectedly.

not result in axial strains in other members. An illustration of the results from a change of the length of the diagonal member is shown. If the number of equations exceeds the degrees of freedom they represent, statically indeterminate modes of self-stress are observed. This is illustrated in Figure 1c. The stresses within the bars are not unique to the nodal displacements, which are over-defined. In terms of creating a stiff structure, one or more of the bars can be considered redundant.

While Maxwell's rule holds true in the majority of cases, it is relatively straightforward to conceive configurations of elements which obey the relations in Equations 1 and 2, but behave unexpectedly. Figure 2 illustrates two such examples. The first, Figure 2a has both regions of static and kinematic indeterminacy while still satisfying equation 2. Figure 2b also obeys Maxwell's rule but has an infinitesimal mechanism, and is only stiff as the structure undergoes displacement. The infinitesimal nature of this mechanism can be shown to be caused by the interaction between the modes of kinematic and static indeterminacy within the structure [5].

Pellegrino and Calladine [5] showed that to fully understand the properties of a framework, the whole geometry needs to be considered, rather than just the number of the elements and connections. By analysing the four vector subspaces of the equilibrium matrix  $A$ , which relates tensions in the bars  $t$  to external nodal forces  $f$  as

$$At = f \tag{3}$$

and also by inspection of its transpose, the kinematic matrix  $B$  which relates the nodal displacements  $u$  to bar elongations  $g$  as

$$Bu = A^T u = g \tag{4}$$

it is possible to find modes of kinematic and static indeterminacy. The nullspace

of  $A$  corresponds to modes of tension in the structure (states of self-stress) which require no external nodal forces. The left-nullspace of  $A$  indicates nodal displacements which do not result in any elongations of bars – inextensional mechanisms. Pellegrino and Calladine also present a technique for determining whether mechanisms found are finite or if they tighten with displacement [5]. This tightening is clearly detrimental when trying to conceive adaptive structures, and is therefore an important consideration. This structural analysis can be unified under a single framework [6] using a singular value decomposition (SVD) to extract the four linear vector subspaces of  $A$ .

### 3. Extension for rigid-jointed assemblies

All the analysis detailed in the previous section has been performed on pin-jointed assemblies. However, frames of this nature are uncommon in practice mostly being seen in the form of tensegrity, cable-net, and civil engineering structures. If the joints are made rigid, there can be no mechanisms. However, there can still be modes of deformation which require a minimum amount of effort to achieve. These modes of structural compliance in rigid-jointed frames can be thought of as being analogous to mechanisms in their pin-jointed equivalent. Similarly, modes in both cases can be excited through actuation to create predetermined displacements. These modes of compliance also indicate various paths to stable (non-buckling) structural collapse, the implications of which are not discussed in this paper.

A rigid-jointed frame is inherently statically indeterminate, and therefore a full finite element representation is used to determine its properties. The technique used to extract the modes in this paper is general, and is suitable for any finite element discretisation. The method presented uses a well known linear elastic finite element formulation, with shear deformable, one dimensional, ‘Timoshenko’ beam elements. This discretisation suits our need to construct slender frames, and also facilitates analogies with existing frame analysis being drawn. The

105 details of the implementation can be found in Appendix A.1. The derivation is well documented, and can be found in full in Hughes', 'The Finite Element Method' [7].

The standard finite element approach is to construct a stiffness matrix  $K$  which relates nodal displacements  $u$  to external forces  $f$  by

$$Ku = f \tag{5}$$

110 We define compliance informally as the amount of effort needed to create a displacement in a structure. Although compliance is typically the inverse of stiffness,  $K$  is not suitable for analysis to extract modes of compliance as the values in the vector  $f$  are not comparable. In our discretisation, for example, it contains moments and torques as well as forces. To address this, a new approach  
115 is proposed that assembles a quasi-stiffness matrix  $\beta$ . This matrix is similar in function to  $B$  in the pin-jointed case, but it is expanded to include the effects of bending, torsion and shear, as well as the axial strains. Unlike  $K$ , this quasi-stiffness matrix relates nodal displacements and rotations to a single measure of strain energy. In this way, the effort required to produce different displacements  
120 can be directly compared.

### 3.1. Assembly of the quasi-stiffness matrix

Equation 4 relates nodal displacement solely to the axial extension of the elements. In order to account for all the sources of strain, an energy-based approach is used. The strain energy density  $U_{den}$  of a pin-jointed structure, is typically  
125 expressed as

$$U_{den} = \frac{1}{2}D\epsilon^2 \tag{6}$$

where  $\epsilon$  is the axial strain and  $D$  denotes the material and geometric properties, as detailed in Appendix A.1. In a similar fashion to  $B$ , the quasi-stiffness matrix

$\beta$  should relate the nodal displacements to a metric representing the amount of strain in the structure,  $R$ . This is expressed as

$$\beta u = R \quad (7)$$

130 The quasi-stiffness matrix  $\beta$  can be seen as the natural extension of the kinematic matrix – rather than linking nodal displacements solely to axial extension, it relates the displacements to the geometric and material weighted effects of all the strain. An expression for  $R$  can be found by taking the square root of the strain energy. Physically, this is the integral of strain in the structure, weighted  
135 by the material moduli,  $D$ . The density of this function for axial strains is

$$R_{den} = \left(\frac{1}{2}D\right)^{0.5} \epsilon \quad (8)$$

An integration is performed over the entire element which is then divided by square root of the element length, thus ensuring whole element is taken into account while preserving physically meaningful dimensions for  $R$ , i.e. the square root of strain energy. The derivation of  $R$  and hence  $\beta$  for a shear deformable  
140 beam element are given in Equations A.9, A.10 and A.11.

If the displacements are separated into a vector,  $R$  can be expressed in terms of nodal displacements  $u$  and the quasi-stiffness matrix  $\beta$ . For a single beam element this is

$$\beta u = \begin{bmatrix} \beta_b \\ \beta_s \\ \beta_a \\ \beta_t \end{bmatrix} u = R \quad (9)$$

where  $b$ ,  $s$ ,  $a$  and  $t$  correspond to bending, shear, axial and torsional components,  
145 respectively. The matrices  $\beta$  for every element can then be assembled into a large matrix describing the whole structure, with  $m$  elements, and  $n$  degrees of



freedom. Each component of strain is assigned a row to prevent negative and positive contributions of strain values from cancelling. The result is a large, but sparse, matrix  $\beta$ , with each element on subsequent series of columns, and the values in columns corresponding to global degrees of freedom.

$$\begin{array}{c}
 \overbrace{\hspace{10em}}^{6m \times n} \\
 \left[ \begin{array}{cccc}
 \overbrace{\begin{bmatrix} \beta_{b1} \\ \beta_{s1} \\ \beta_{a1} \\ \beta_{t1} \end{bmatrix}}^{6 \times 12} & 0 & \cdots & 0 \\
 0 & \begin{bmatrix} \beta_{b2} \\ \beta_{s2} \\ \beta_{a2} \\ \beta_{t2} \end{bmatrix} & \cdots & 0 \\
 \vdots & \vdots & \ddots & 0 \\
 0 & 0 & 0 & \begin{bmatrix} \beta_{bm} \\ \beta_{sm} \\ \beta_{am} \\ \beta_{tm} \end{bmatrix}
 \end{array} \right] \begin{array}{c}
 \overbrace{\begin{bmatrix} u_1 \\ u_2 \\ \vdots \\ u_n \end{bmatrix}}^{n \times 1} \\
 = \overbrace{\{R\}}^{6m \times 1}
 \end{array} \quad (10)
 \end{array}$$

Once the matrix  $\beta$  is assembled, the modes of compliance can be extracted through a singular value decomposition.

### 3.2. Singular Value Decomposition

The implementation and the derivation of the SVD is beyond the scope of this paper, but it is well documented in other sources [8]. For the work presented in this paper, the decomposition was carried out using the ‘svd’ function in

MATLAB [9]. The matrix  $\beta$  is factorised into three matrices

$$\overbrace{[\beta]}^{6m \times n} = \overbrace{[Q]}^{6m \times 6m} \overbrace{[S]}^{6m \times n} \overbrace{[V^T]}^{n \times n} \quad (11)$$

Where  $Q$  and  $V$  are unitary matrices, and  $S$  is an ordered diagonal matrix of non-negative numbers. The columns of  $Q$  and  $V$  are orthogonal. In the context of  $\beta$ , the columns of  $Q$  are the basis vectors which span the structural strain space of the structure, and the columns of  $V$  are basis vectors which span the nodal displacement space. As the basis vectors are unit vectors, the values in  $S$  indicate the effort needed to produce each orthogonal displacement. As  $S$  is ordered, so too are the modes of deformation of the structure. The formulation of  $R$  in Equation A.10 results in the values in  $S$  indicating the square root of the energy required to produce a given mode.

This process is similar to finding the inextensible mechanisms and states of self-stress from the nullspace and left-nullspace of  $A$ . Instead of finding vectors of nodal displacement that result in zero bar elongations or vectors of bar tensions with no external forces, unit vectors of nodal displacement which result in minimum effort are found.

#### 4. Linear compliant modes

For example, if a two dimensional portal frame, as illustrated in Figure 3, is pin-jointed there is a clear mode of kinematic indeterminacy. When the joints become rigid, the various modes of compliance can be extracted, according to the procedure in the previous section. In this example, the structure is comprised of slender members of 1 unit in length, and each having a square cross section with an edge length of  $1 \times 10^{-3}$  units.

Figure 3b clearly shows how a mode of compliance in a slender structure can be a facsimile of an inextensible mechanism. The rotations at the joints have

been replaced with bending of the bars – by far the most energy efficient way to achieve a displacement, discounting any distal effects of torsion. This effect is pronounced due to the slender nature of the structure. This pattern is continued into the higher modes, with an increase in the total curvature of the structure  
 185 leading to the higher strain energies.

While this example is straightforward, and the mode-shapes are intuitive, the same principles can be applied to more complex structures giving crucial insight into how mechanisms can be directly and efficiently replaced by compliance, with the nodal rotations imitated by bending deformation. The associated energy  
 190 cost of this substitution, for a given material and geometry and can also be easily quantified from the values in  $S$ . Crucially, an appreciation for the other, potentially undesirable, modes of compliance which are being introduced is also

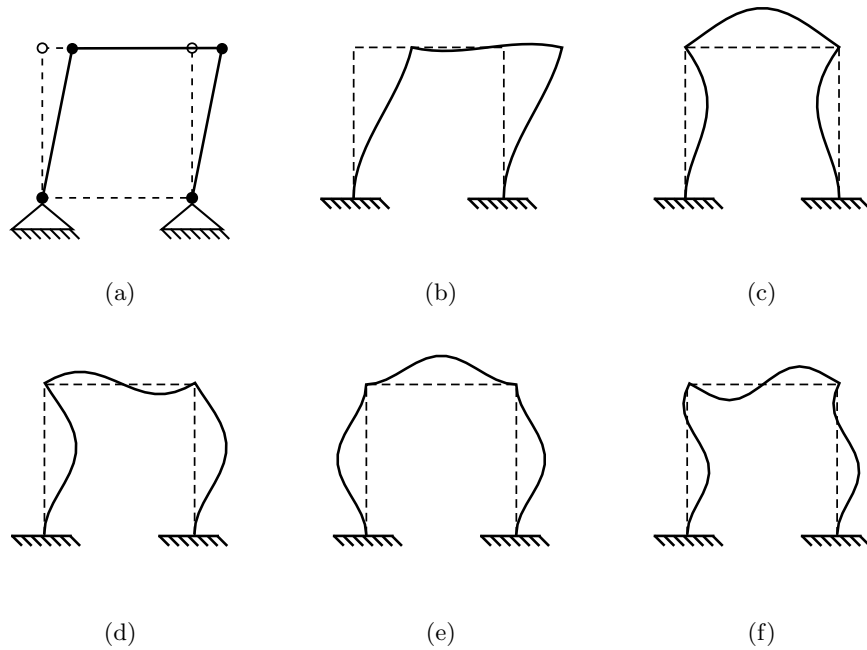


Figure 3: A mode of kinematic indeterminacy when the structure is pin-jointed is shown in 3a. Figures 3b to 3f show the five modes of greatest compliance when the joints are rigid, for a two dimensional portal frame.

gained. By altering the geometry, certain modes can be prioritised. A simple example of this would be to change the aspect ratio of the sections of a planar structure to increase the energy required to produce out-of-plane modes, and therefore ensure an in-plane mode is excited under actuation, or vice-versa.

All the modes considered so far have been linear, which is reasonable for small displacements, however, for many practical adaptive structure applications large displacements are required. These larger displacement can mean geometric nonlinearities become relevant, leading to undesired tightening or self-stiffening of the structure.

## 5. Accounting for nonlinearities

The structure shown in Figure 3, and its associated mode shapes, are not heavily influenced by any geometric nonlinearity. However, all linear bending analysis results in elongation of members, the energy cost of which is not taken into account. This results in an under-prediction of the total effort required to generate the displacement mode shapes, when the displacements are large. For true deformations to be determined, for a given input, these effects need to be captured.

An appreciation of the impact of these second order effects is also important when considering a structure for actuation. By drawing an analogy with pin-jointed frames, this is equivalent to differentiating between finite and infinitesimal modes of kinematic indeterminacy. If the mechanisms tighten with displacement, they do not make efficient modes of actuation. For pin-jointed frames, this first order stiffening can be found by looking at the interactions between modes of kinematic and static indeterminacy [5]. However, if the framework is rigid jointed it is inherently indeterminate, with many irrelevant modes of self-stress, and therefore another approach is needed.

In order to account for the nonlinearities, an iterative approach is used. A schematic illustration of this method for a one-degree-of-freedom case is shown

in Figure 4. The aim is to find the nonlinear displacements, which are achieved using the same vector  $R$  as the initial linear mode, indicated by the star.  $R_{linear}$  is found using equation 9, and the linear displacement mode of interest, a column of the matrix  $V$ , is obtained through factorisation of  $\beta$ . The linear analysis does not capture higher order effects, such as the elongation of members due to bending. This is addressed by recalculating  $\beta$  using an updated geometry half-way between the deformed and undeformed case ( $\beta_2$ ).  $R_2$  is then found as twice of the square-root of the energy required to return the structure to the undeformed case from the geometry used to calculate ( $\beta_2$ ). This is equivalent to finding the square-root of the strain energy required to move to the deformation  $u_{linear}$  using the average linear approximation to the tangential quasi-stiffness. The second order effects are captured by taking into account the changing quasi-stiffness over the deflection. As  $R_{linear}$  is known, the root energy vector  $R_3$  can then be found to return to the same energy state as the linear mode, where  $R_3 = (R_{linear} - R_2)$ . To find the displacements, an SVD of  $\beta_2$  is taken

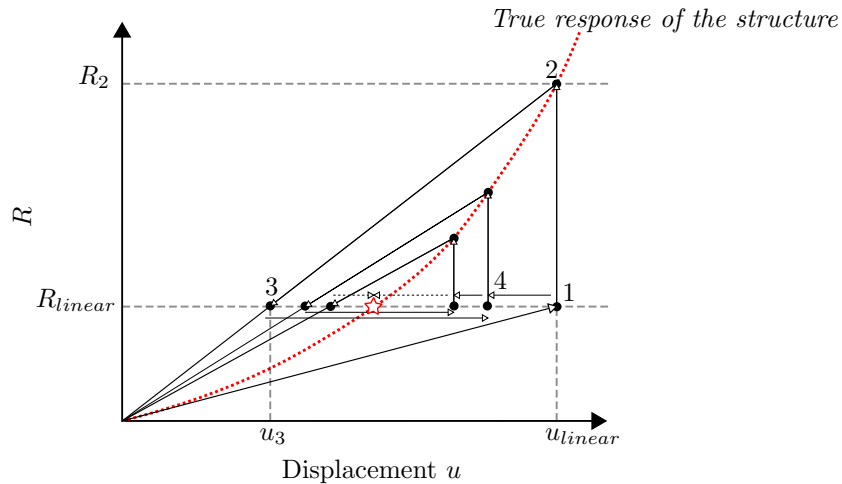


Figure 4: A schematic illustration of the iterative process used to account for nonlinear effects, in a one-degree-of-freedom system. The displacement of the structure is found, indicated by the star, where the nonlinear deformation takes the same energy as predicted by the linear mode. This energy vector is denoted by  $R_{linear}$ .

$$\beta_2 = Q_2 S_2 V_2^T \quad (12)$$

This decomposition is then used to find the pseudo-inverse of  $\beta_2$ , and hence the displacements  $u_3$  at point 3 in Figure 4 are found when the root energy vector  $R_3$  is applied to  $\beta_2^+$ , expressed as

$$u_3 = \beta_2^+ R_3 = V_2 S_2^+ Q_2^T R_3 \quad (13)$$

The new displacement  $u_3$  is then used to apply an improvement to the linear displacement  $u_{linear}$ , and point 4 in Figure 4 is found. This process is then repeated until a satisfactory level of convergence is achieved. It is often not possible for the nonlinear correction to converge to a solution that has the same energy as  $R_{linear}$ , indicating an irreparable under-prediction of energy expenditure by the linear deformation, indicative of tightening of the structure under actuation. A fully converged solution results in deflections  $u$  which take the same magnitude of  $R$  to produce as required to return the deformed structure back to its initial configuration.

## 6. Compliant modes examples

The matrix analysis detailed above, as well as the correction for the effects of strain stiffening caused by nonlinear deformations can be applied to find the most efficient way to actuate a structure. A simple test case is a three dimensional ‘h-frame’, with built in boundary conditions at either end, as displayed in Figure 5.

### 6.1. Built in h-frame

The spherical-jointed h-frame has three modes of kinematic indeterminacy, as illustrated in Figures 6i, 6j and 6k. Two of these modes tighten with displacement, and one can move freely. The structure considered is 3 units in length,

with a square cross section of  $1 \times 10^{-2}$ , resulting in a slender frame. This slenderness in turn results in bending dominated modes of compliance being ‘inherited’ from the spherical-jointed case, when the joints are made rigid. This occurs as the result of rotations previously produced at the nodes being generated instead through rotation via bending. It is clear that, in practice, many of these modes would not be suitable for actuation. The deformations shown in Figures 6b, 6c and 6d require significant elongation of the bars. By implementing the nonlinear correction, it is shown that only the first mode can achieve any significant displacement. This is to be expected, as the first mode has parallels with the finite inextensible mechanism. The h-frame is a simple structure, and although the most efficient way to create a deformation is intuitive, it illustrates the importance of considering nonlinearities, while ratifying the general approach. The same process can be applied to a more complex geometry, with a greater scope as an adaptive structure.

### 6.2. Finite Kagome lattice

The Kagome lattice geometry is well known for possessing some unique and useful actuation properties. It has been used previously to create optimal actuated sandwich-like structures, capable of producing out-of-plane [10, 11] and in-plane [12] waveforms, with members of the framework replaced by, or at-

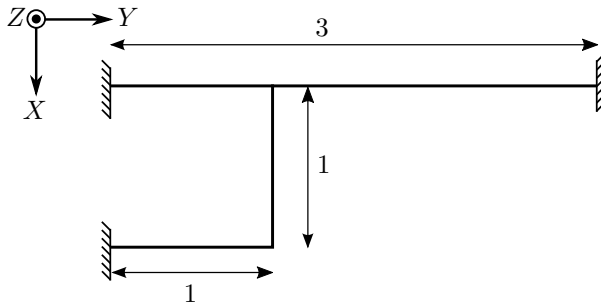


Figure 5: A simple ‘h’ shaped structure, fixed in place with built in boundary conditions. The dimensions of the structure are displayed. The cross-section is square with a width of  $1 \times 10^{-2}$ , producing a slender structure.

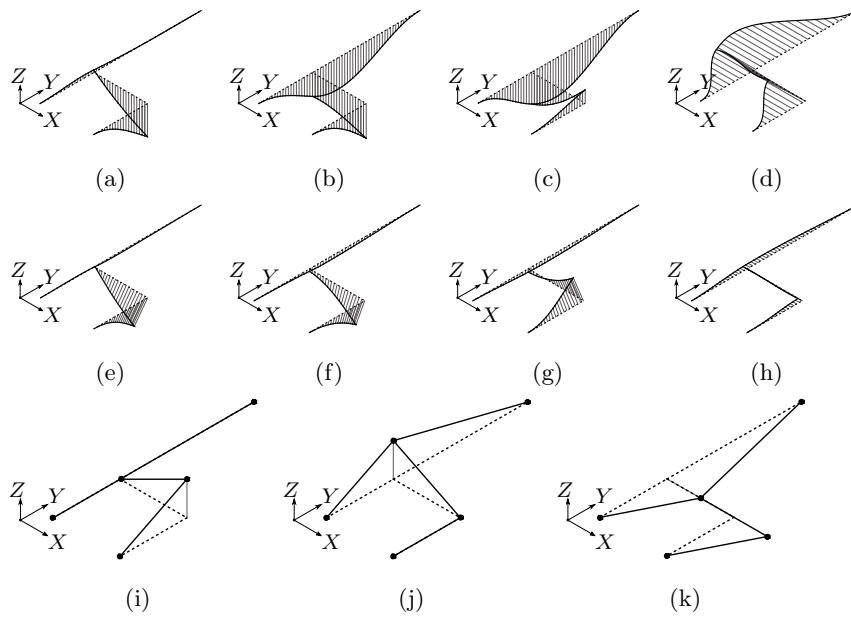


Figure 6: The first 4 linear modes of compliance of the structure in Figure 5 are shown in Figures 6a, 6b, 6c and 6d while Figures 6e, 6f, 6g and 6h show the same modes corrected for nonlinear effects. If the structure is assumed have spherical-joints and rotation permitting boundary conditions, then Figure 6i displays the only mode of finite kinematic indeterminacy. The two modes representing infinitesimal mechanisms are shown in Figures 6j and 6k.



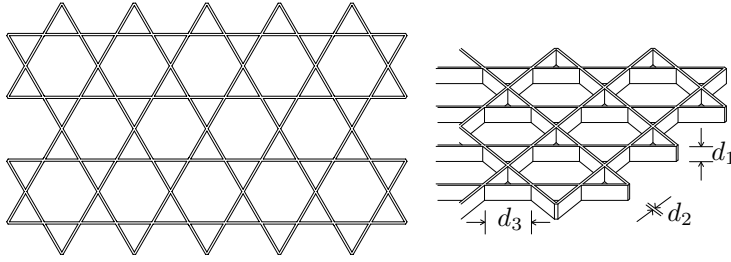


Figure 7: A finite rigid-jointed kagome lattice structure, with a fixed number of unit cells. The internal geometry is parametrised in terms of bar height  $d_1$ , thickness  $d_2$ , and length  $d_3$ .

tached to, actuators. The geometry has also been considered numerically as an infinite, or large, planar lattice [13, 14]. In this configuration, it has been shown that macroscopic deformations can be produced efficiently within the structure, with the actuation of a single bar. The modes of kinematic indeterminacy lead to a structure which transmits actuations along discrete ‘corridors’. This has practical applications for creating efficient adaptive structures, as large controlled fields of deformation can be created with very few actuators.

If the pin-jointed Kagome lattice is considered infinite, it can not be both kinematically and statically determinate [15]. In this case, the modes of self-stress impinge on the modes of kinematic indeterminacy, causing them to become infinitesimal. This interaction naturally reduces the ability of the structure to propagate an actuation. If the structure is finite and free-floating it becomes statically determinate, and with careful selection of boundary conditions it can be supported while preventing self-stress within the structure.

For a practical application, a finite free-floating structure is considered, and illustrated in Figure 7. With pin joints at the nodes, this structure has 93 modes of kinematic indeterminacy, and 6 rigid body modes. With no boundary conditions there are no states of self stress, and consequently all inextensible mechanisms are finite [5]. Four of these modes of kinematic indeterminacy are displayed in Figure 8. These orthogonal modes illustrate how the pin-jointed structure can produce discrete areas of in-plane displacement, under actuation.

In order to create a rigid structure with the propensity to produce this in-plane displacement, the structure was parametrised as indicated in Figure 7, in terms of characteristic lengths  $d_1$ ,  $d_2$  and  $d_3$ . The general geometry of the structure was unaltered. A brief parametric study was performed, and linear modes of compliance were extracted, and the actuation effort was found. The aspect ratio, defined as  $\frac{d_1}{d_2}$  and the stockiness of the structure, defined as  $\frac{\sqrt{d_1 d_2}}{d_3}$  were varied. The actuation effort, taken from the matrix  $S$  in Equation 11 and scaled with  $d_3$ , is displayed in Figure 9.

As the structure becomes less stocky, the actuation requirements for a given aspect ratio decreases. The increasingly efficient bar bending with slenderness causes the structure to tend towards the pin-jointed case, with the nodal rotations being replaced with rotation through bending. For a given stockiness, as aspect ratio increases, so does the energy required to deform the structure. In this case, this trend continues until the aspect ratio  $\approx 11$ . While the aspect ratio is less than this value, out-of-plane modes are easier to produce, but above this threshold, the structure is easier to deform in-plane. This property is enhanced with increased aspect ratio. Interestingly, the flip between in-plane and out-of-plane displacements is independent of stockiness, and is only a function of the aspect ratio of the cross-section.

Two such modes are shown in Figure 10. The first is an out-of-plane mode when the aspect ratio is 1. The second is an in-plane mode when the aspect ratio is  $\approx 160$ . Also shown is the in-plane mode with the correction for nonlinear effects applied. Figure 10a illustrates that the out-of-plane mode is similar

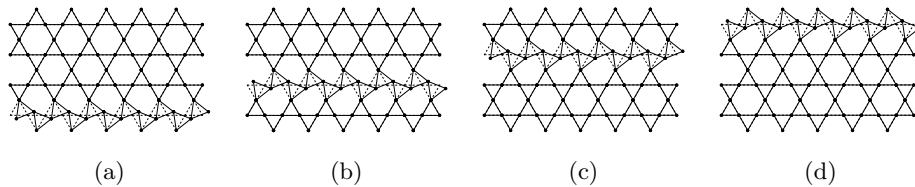


Figure 8: Four modes of kinematic indeterminacy, indicating finite inextensible mechanisms for a finite free floating Kagome structure.

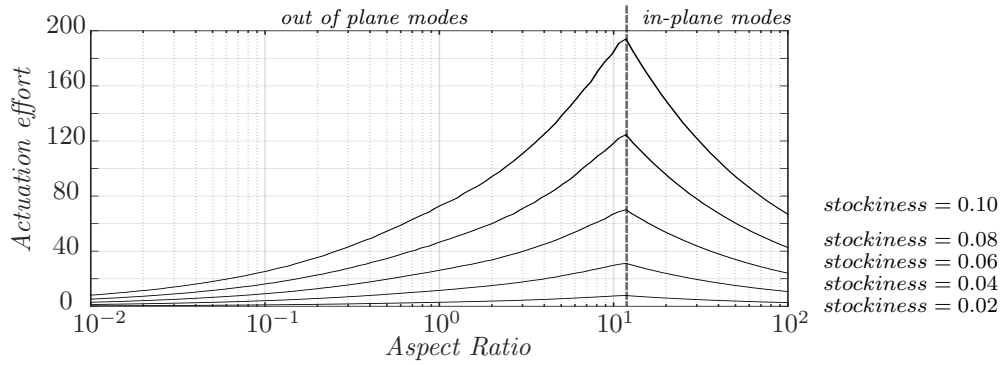


Figure 9: A graph illustrating how actuation effort varies with aspect ratio and stockiness for a finite Kagome lattice structure, as displayed in Figure 7. In-plane modes dominate above an aspect ratio of 10

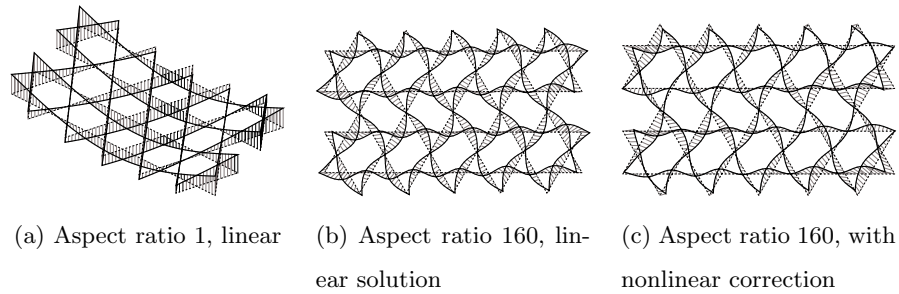


Figure 10: Three low actuation effort mode shapes with varying aspect ratio, showing transition between out-of-plane and in-plane preferred modes.

to plate bending, and the internal geometry of the structure appears to have little bearing on the deformation. The in-plane displacements in Figure 10b are similar to the mechanisms seen in Figure 8. When the nonlinearities are taken into account, shown in Figure 10c the displacements are preserved. The lack of boundary conditions prevents the ‘corridors’ of displacement from being hindered, as predicted by the lack of infinitesimal mechanisms in the pin-joined analysis. The nonlinear correction shows how the structure is pulled in towards the center, and therefore indicates that any boundary conditions applied to the structure must facilitate these motions to allow for easy actuation.

330 The study also yields other useful information when designing this structure for  
in-plane actuation. For example, the bars should be as slender as feasible, with  
an aspect ratio greater than 11. Analysing the structure in terms of modes of  
compliance is a natural way of designing for actuation, as it yields the innate  
behaviour of a given structural geometry. The same kind of parametric study  
335 could be performed by applying a force to the structure and assessing the fidelity  
of the deformation and associated stresses, or by calculating the various bucking  
modes. However, in both these cases, a location for the forces needs to be  
prescribed or treated as variables, as do the boundary conditions. The response  
to a load would also not capture the propensity of the structure to deform out-  
340 of-plane, or in an unexpected way, at least not without some structural defects  
being imposed *a priori*. A buckling analysis, in many cases, would also be  
inappropriate as deformation even under large actuation displacements, is often  
governed by nonlinear bending rather than an instability. By considering the  
nature of the structure, and designing it such that certain modes are encouraged,  
345 an efficient active structure can be created.

This process can be refined through manipulation of certain modes, rather than  
a computationally-expensive parametric study or optimisation routine. By look-  
ing at the modes, the properties of individual bars can be chosen to facilitate  
the desired deformation, without having to treat each as a variable in an opti-  
350 misation routine. The Kagome geometry, as illustrated in Figure 7 is used again  
as a test case, but in practice this method is most powerful when the structure  
considered is irregular, and can not be parameterised efficiently.

## 7. Modal optimisation

In the case of the Kagome lattice structure, we aim to produce a continu-  
355 ous structure capable of imitating the four pin-jointed mechanisms shown in  
Figure 8. Importantly, a structure which inhibits out-of-plane deformations is  
also required. The initial structure, as displayed Figure 7, with feasible but

essentially arbitrary values for  $u$ , and material properties is factorised, as in Equation 11.

360 The matrix  $V$  yields the modes of compliance of the structure, ranked in order of how easily they are produced. The modes relevant to the application can be selected in a number of ways, through physical intuition if the problem is straightforward, or through numerical comparison to a desired deformation for more complex cases. As the columns of  $V$  span the displacement space of the  
 365 structure, a weighted sum of modes will be able to replicate any deformation.

As the desired deformations are known, and only low energy modes are of interest, an approximation using a reduced modal model to approximate the target displacements  $u_t$  can be expressed as

$$\overbrace{\left[ V_r \right]}^{n \times c} \overbrace{\left\{ \omega \right\}}^{c \times 1} = \overbrace{\left\{ u_t \right\}}^{n \times 1} \quad (14)$$

where  $V_r$  is a sub-set of  $V$ , comprising the low energy modes, and  $\omega$  is the  
 370 proportion each of the modes contribute to the displacements in  $u_t$ . The number of modes selected is indicated by  $c$ , typically the ones corresponding to the lowest values in  $S$ . In this way, by setting  $u_t$  to various desired displacements it is possible to see which modes need to be encouraged, and conversely, which modes need to be suppressed and to what degree. Producing a reduced version  
 375 of  $V$  both makes finding  $\omega$  easier, and also means that only low-energy modes are considered. By using only these modes, the number of degrees of freedom upon which  $\omega$  is selected can also be reduced, as irrelevant structural deformations of high wave number will not be considered.

For each of the displacement modes in  $V$ , there is a corresponding stress mode  
 380 as a column in  $Q$ . This column is equivalent to the normalised vector of  $\beta$  multiplied by that displacement mode.  $Q_r$  is a matrix consisting of the stress states of the displacements modes in  $V_r$ . If there are  $p$  desired and  $q$  undesired

displacements vectors  $u_t$ , the cumulative effect can be expressed as

$$e = \frac{h_p}{p} \sum_{i=1}^p Q_r |\omega_i| + \frac{h_q}{q} \sum_{j=1}^q Q_r |\omega_j| \quad (15)$$

where  $e$ , the stiffness improvement vector, describes how the stiffness of each  
 385 element of the structure needs to change to reflect the modes enhanced and sup-  
 pressed. Constants  $h_p$  and  $h_q$  determine how the modes selected are enhanced  
 or attenuated, respectively. By having  $h_p = 0.1$  and  $h_q = 10$ , for example,  
 would result in 2 orders of magnitude difference in ease of actuation between  
 the unwanted and the favoured mode shapes for actuation.  $\beta$  is constructed in  
 390 such a way that  $e$  can be broken down into values for each element, as well as  
 for each source of stiffness as

$$e = \left\{ \overbrace{\left\{ \left( e_{b1} \right) \left( e_{s1} \right) \left( e_{a1} \right) \left( e_{t1} \right) \right\}}^{\text{element 1}} \overbrace{\left\{ \left( e_{b2} \right) \left( e_{s2} \right) \left( e_{a2} \right) \left( e_{t2} \right) \right\}}^{\text{element 2}} \right. \\ \left. \dots \overbrace{\left\{ \left( e_{bm} \right) \left( e_{sm} \right) \left( e_{am} \right) \left( e_{tm} \right) \right\}}^{\text{element } m} \right\} \quad (16)$$

where the subscripts relate to source of the stress (bending, shear, axial and  
 torsional), as well as the element number. The element properties, the values  
 in matrix  $D$  given in Equation A.5, can then be adjusted for each element.  
 395 Sometimes it might not be feasible to alter the material properties, or certain  
 element dimensions, leading to a trade off between components of stiffness. For  
 example, if the out-of-plane height of the elements,  $d_1$  were kept constant, axial  
 stiffness might have to decrease to allow in-plane bending stiffness to decrease,  
 even if this change is not explicitly prescribed in  $e$ . The improved geometric  
 and material properties,  $D_{new}$  can be found from  $e$ , and the initial values of  $D$   
 400 by solving

$$D_{new} = De \tag{17}$$

where  $D$  is calculated for the initial structure.

When the structure in Figure 7 with an aspect ratio of 1, and a stockiness of 0.016, is analysed using this method, four key modes displayed in Figure 11 are selected, as their weighted sum replicates all of the modes in Figure 8. The modal number corresponds to their ranking, in terms of ease to produce as deformations in the original structure. It is clear that the initial structure has no propensity to mimic the modes in Figure 10, as the in-plane modes fall high up in the rank.  $D_{new}$  was found by altering only the element thickness, using  $h_p = 0.1$  and  $h_q = 10$ . Consequently, the in-plane thickness of the members of the structure are reduced considerably, producing a mean aspect ratio of  $\approx 90$ . This corroborates with the results of the parametric study, displayed in Figure 9. Furthermore, when the weighting to the modes is applied to  $Q$ , and reassembled into a new  $\beta$ , with  $S$  and  $V$  and re-factorised, the modes displayed in Figure 11 are found to be ranked as the four easiest to produce, indicating that the nature of the structure has changed favorably. Reordering specific modes of compliance through manipulating the structural properties of the elements, by producing a reduced-model, is a very efficient way to design compliant structures. Performing the SVD has by far the largest computational cost, but only needs to be done once as the basis vectors extracted offer a complete description of the geometry. In this way, the structure can be efficiently honed to have the desired compliance and performance under actuation.

## 8. Conclusions

Considering structures for actuation is typically done in terms of applied forces, boundary conditions and displacements. In this paper, we have proposed a new method using a modal decomposition of the structure to extract inherent modes

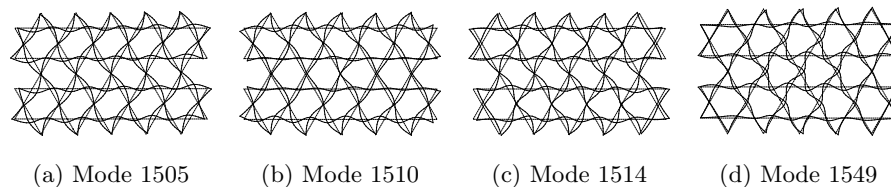


Figure 11: Four modes which can be summed to give a good approximation to the four ‘corridors’ of actuation in Figure 8. The mode number corresponds to the ranking of the mode, in terms of actuation effort, in the original structural design.

of compliance. These modes are found through a singular value decomposition of a quasi-stiffness matrix  $\beta$ , assembled using a strain energy approach. A reduced model of the structure, using only of relevant orthogonal modes, is then  
 430 constructed. By enhancing or attenuating certain modes, an efficient process for optimising compliant structures is outlined. The Kagome lattice geometry, known for its favourable actuation characteristics, is used to demonstrate the approach. The method is implemented throughout with a beam-element model.

Nonlinear effects known to inhibit mechanisms in pin-jointed frames are shown  
 435 to display similar effects in the analysis of compliant structures. Both tightening of the structure under finite displacements, due to the structure impinging upon itself, as well as the first order effects of bending under large deflections is not captured with the linear analysis. An iterative scheme is presented to adjust the linear modes to take these nonlinear phenomena into account.

440 The processes detailed in this paper give a new way to consider adaptive structures in terms of innate modes of compliance. It also demonstrates how the manipulation of these modes can form the basis of an efficient structural optimisation routine.

## 9. Acknowledgements

445 The authors would like to gratefully acknowledge Airbus Group Innovations who funded the work presented in this paper, under agreement IW202838.



## Appendix A. Beam element description

### Appendix A.1. Finite element discretisation

As the finite element scheme used is well known, well documented, and quite simple only the salient details are presented. One-dimensional prismatic beam elements are used, with linear basis functions, as in Equation A.1. The element and associated coordinate systems are defined in Figure A.12. A superscript  $e$  indicates that the variables apply to the element, rather than global system.  $x_{1-3}$  signify the coordinate systems,  $\theta_{1-6}$  rotations, and  $w_{1-6}$  displacements. The dimensions of the element are expressed with the variable  $d_{1-3}$ . The two basis functions in terms of  $x^e$  and denoted by  $N$  are

$$\begin{aligned} N_1 &= 1 - \frac{x_3^e}{d_3} \\ N_2 &= \frac{x_3^e}{d_3} \end{aligned} \tag{A.1}$$

Using these shape functions, and following the procedure laid out in Hughes [7],  
 450 element deformation matrices for bending  $P_b$ , shear  $P_s$ , axial  $P_a$ , and torsional  
 $P_t$  strain can be composed

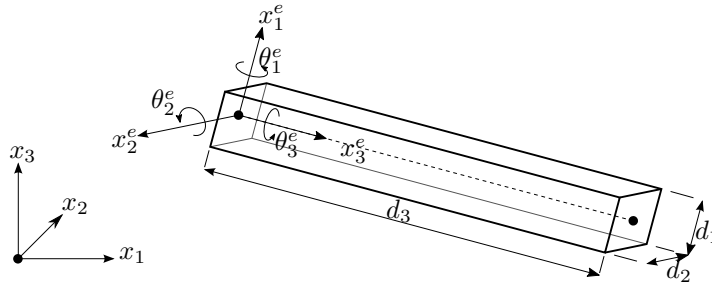


Figure A.12: A single prismatic beam element illustrating the global and elemental coordinate systems  $x$ , the dimensions of the element  $d$ , and the nodal displacements and rotations,  $w$  and  $\theta$ , respectively.

$$\begin{aligned}
P_b &= \begin{bmatrix} 0 & 0 & 0 & \frac{dN_1}{dx_3} & 0 & 0 & 0 & 0 & 0 & \frac{dN_2}{dx_3} & 0 & 0 \\ 0 & 0 & 0 & 0 & \frac{dN_1}{dx_3} & 0 & 0 & 0 & 0 & 0 & \frac{dN_2}{dx_3} & 0 \end{bmatrix} \\
P_s &= \begin{bmatrix} \frac{dN_1}{dx_3} & 0 & 0 & 0 & \frac{-N_1}{dx_3} & 0 & \frac{dN_2}{dx_3} & 0 & 0 & 0 & \frac{-N_2}{dx_3} & 0 \\ 0 & \frac{dN_1}{dx_3} & 0 & \frac{N_1}{dx_3} & 0 & 0 & 0 & \frac{dN_2}{dx_3} & 0 & \frac{N_2}{dx_3} & 0 & 0 \end{bmatrix} \\
P_a &= \begin{bmatrix} 0 & 0 & \frac{dN_1}{dx_3} & 0 & 0 & 0 & 0 & 0 & \frac{dN_2}{dx_3} & 0 & 0 & 0 \end{bmatrix} \\
P_t &= \begin{bmatrix} 0 & 0 & 0 & 0 & 0 & \frac{dN_1}{dx_3} & 0 & 0 & 0 & 0 & 0 & \frac{dN_2}{dx_3} \end{bmatrix}
\end{aligned} \tag{A.2}$$

The 12 degrees of freedom for each element, in the element coordinate system, can be assembled into the vector  $u^e$  with the subscripts 1 – 3 corresponding to the first node, and 4 – 6 the second.

$$u^e = \left\{ w_1^e \quad w_2^e \quad w_3^e \quad \theta_1^e \quad \theta_2^e \quad \theta_3^e \quad w_4^e \quad w_5^e \quad w_6^e \quad \theta_4^e \quad \theta_5^e \quad \theta_6^e \right\}^T \tag{A.3}$$

455 The various strains within an element for a given nodal displacement,  $u^e$  can be found from the element deformation matrices by

$$\begin{aligned}
\kappa^e &= P_b u^e \\
\gamma^e &= P_s u^e \\
\epsilon^e &= P_a u^e \\
\psi^e &= P_t u^e
\end{aligned} \tag{A.4}$$

where  $\kappa$ ,  $\gamma$ ,  $\epsilon$  and  $\psi$  represent the bending, shear, axial and torsional strains, respectively. The standard finite element approach is to integrate the element deformation matrices, multiplied by the material moduli matrices  $D$  which can

460 be expressed as

$$\begin{aligned}
D_b &= \begin{bmatrix} EI_1 & 0 \\ 0 & EI_2 \end{bmatrix} \\
D_s &= \begin{bmatrix} \mu a \phi & 0 \\ 0 & \mu a \phi \end{bmatrix} \\
D_a &= [Ea] \\
D_t &= [\mu I_3]
\end{aligned} \tag{A.5}$$

in order to construct an elemental stiffness matrix  $k^e$ . Where  $E$  is the Young's modulus and  $I_{1-2}$  refer to the second moment of area, calculated from  $d_1$  and  $d_2$ . The cross-sectional area is denoted by  $a$ , with a correction factor  $\phi$  [16] required to correct for the distribution of shear strain across the section, with  $\mu$  being the shear modulus.  $I_3$  is the polar moment of inertia of the beam around  $x_3^e$ . Hence,  $k^e$  can be found as

$$k^e = \int_0^{d_3} P_b^T D_b P_b + P_s^T D_s P_s + P_a^T D_a P_a + P_t^T D_t P_t dx_3^e \tag{A.6}$$

In order to move between the coordinate system of an element, and the global coordinate system of the structure, a rotation matrix  $T^e$  is required. If  $t^e$  is the  $3 \times 3$  matrix which transforms the basis vectors  $x^e$  to  $x$  as illustrated in Figure A.12, then for the 12 degrees of freedom of the element,  $T^e$  can be expressed as

$$T^e = \begin{bmatrix} t^e & 0 & 0 & 0 \\ 0 & t^e & 0 & 0 \\ 0 & 0 & t^e & 0 \\ 0 & 0 & 0 & t^e \end{bmatrix} \tag{A.7}$$

such that  $k = T^e k^e T^{eT}$ , and  $W = T^e W^e$ , for example. The construction of the global stiffness matrix  $K$  forms the backbone of linear finite element analysis,

relating the displacements  $u$  with nodal forces  $f$  as

$$Ku = f \quad (\text{A.8})$$

475 *Appendix A.2. Assembly of the quasi-stiffness matrix*

While the goal of the previous section is the assembly of the matrix  $K$ , a quasi-stiffness matrix  $\beta$  is needed to determine modes of compliance. As in Equation 7,  $\beta u = R$  can be found as

$$\begin{aligned} R_b^e &= \left( \frac{D_b}{2d_3} \right)^{0.5} \int_0^{d_3} \kappa \, dx_3 = \left( \frac{D_b}{2d_3} \right)^{0.5} \int_0^{d_3} (P_b u^e) \, dx_3 \\ R_s^e &= \left( \frac{D_s}{2d_3} \right)^{0.5} \int_0^{d_3} \gamma \, dx_3 = \left( \frac{D_s}{2d_3} \right)^{0.5} \int_0^{d_3} (P_s u^e) \, dx_3 \\ R_a^e &= \left( \frac{D_a}{2d_3} \right)^{0.5} \int_0^{d_3} \epsilon \, dx_3 = \left( \frac{D_a}{2d_3} \right)^{0.5} \int_0^{d_3} (P_a u^e) \, dx_3 \\ R_t^e &= \left( \frac{D_t}{2d_3} \right)^{0.5} \int_0^{d_3} \psi \, dx_3 = \left( \frac{D_t}{2d_3} \right)^{0.5} \int_0^{d_3} (P_t u^e) \, dx_3 \end{aligned} \quad (\text{A.9})$$

which when expressed in the global coordinate system becomes

$$\begin{aligned} R_b &= \left( \frac{D_b}{2d_3} \right)^{0.5} \int_0^{d_3} (P_b (T^e)^T u) \, dx_3 \\ R_s &= \left( \frac{D_s}{2d_3} \right)^{0.5} \int_0^{d_3} (P_s (T^e)^T u) \, dx_3 \\ R_a &= \left( \frac{D_a}{2d_3} \right)^{0.5} \int_0^{d_3} (P_a (T^e)^T u) \, dx_3 \\ R_t &= \left( \frac{D_t}{2d_3} \right)^{0.5} \int_0^{d_3} (P_t (T^e)^T u) \, dx_3 \end{aligned} \quad (\text{A.10})$$

480 in which the subscripts  $b$ ,  $s$ ,  $a$  and  $t$  correspond to bending, shear, axial and torsional contributions to  $R$ , respectively.

If the integration is performed analytically, and linear shape functions are used, the individual element components of the quasi-stiffness matrix become

$$\begin{aligned}
\beta_b &= \left(\frac{D_b}{2}\right)^{0.5} \begin{bmatrix} 0 & 0 & 0 & \frac{-1}{\sqrt{d_3}} & 0 & 0 & 0 & 0 & 0 & \frac{1}{\sqrt{d_3}} & 0 & 0 \\ 0 & 0 & 0 & 0 & \frac{-1}{\sqrt{d_3}} & 0 & 0 & 0 & 0 & 0 & \frac{1}{\sqrt{d_3}} & 0 \end{bmatrix} (T^e)^T \\
\beta_s &= \left(\frac{D_s}{2}\right)^{0.5} \begin{bmatrix} \frac{-1}{\sqrt{d_3}} & 0 & 0 & 0 & \frac{-\sqrt{d_3}}{2} & 0 & \frac{1}{\sqrt{d_3}} & 0 & 0 & 0 & \frac{-\sqrt{d_3}}{2} & 0 \\ 0 & \frac{-1}{\sqrt{d_3}} & 0 & \frac{-\sqrt{d_3}}{2} & 0 & 0 & 0 & \frac{1}{\sqrt{d_3}} & 0 & \frac{\sqrt{d_3}}{2} & 0 & 0 \end{bmatrix} (T^e)^T \\
\beta_a &= \left(\frac{D_a}{2}\right)^{0.5} \begin{bmatrix} 0 & 0 & \frac{-1}{\sqrt{d_3}} & 0 & 0 & 0 & 0 & 0 & \frac{1}{\sqrt{d_3}} & 0 & 0 & 0 \end{bmatrix} (T^e)^T \\
\beta_t &= \left(\frac{D_t}{2}\right)^{0.5} \begin{bmatrix} 0 & 0 & 0 & 0 & 0 & \frac{-1}{\sqrt{d_3}} & 0 & 0 & 0 & 0 & 0 & \frac{1}{\sqrt{d_3}} \end{bmatrix} (T^e)^T
\end{aligned} \tag{A.11}$$

These individual components are then assembled into a larger matrix, as in Equation 10, which then forms the basis of the analysis.

485 **References**

- [1] L. L. Howell, *Compliant mechanisms*, John Wiley & Sons, 2001.
- [2] S. D. Guest, S. Pellegrino, The Folding of Triangulated Cylinders, Part II: The Folding Process, *Journal of Applied Mechanics* 61 (4) (1994) 778.
- [3] M. Santer, S. Pellegrino, Topological Optimization of Compliant Adaptive Wing Structure, *AIAA Journal* 47 (3) (2009) 523–534.
- 490
- [4] J. C. Maxwell, On the calculation of the equilibrium and stiffness of frames, *Philosophical Magazine Series 4* 27 (182) (1864) 294–299.
- [5] S. Pellegrino, C. Calladine, Matrix analysis of statically and kinematically indeterminate frameworks, *International Journal of Solids and Structures* 22 (4) (1986) 409–428.
- 495
- [6] S. Pellegrino, Analysis of prestressed mechanisms, *International Journal of Solids and Structures* 26 (I) (1990) 1329–1350.
- [7] T. J. R. Hughes, *The finite element method: linear static and dynamic finite element analysis*, Courier Dover Publications, 2012.
- [8] K. F. Riley, M. P. Hobson, S. J. Bence, *Mathematical methods for physics and engineering: a comprehensive guide*, Cambridge University Press, 2006.
- 500
- [9] MATLAB, Version: 8.3.0.532 (R2014a), The MathWorks Inc., 2014.
- [10] D. Symons, R. Hutchinson, N. Fleck, Actuation of the Kagome Double-Layer Grid. Part 1: Prediction of performance of the perfect structure, *Journal of the Mechanics and Physics of Solids* 53 (8) (2005) 1855–1874.
- 505
- [11] D. D. Symons, J. Shiek, N. Fleck, Actuation of the Kagome Double-Layer Grid. Part 2: Effect of imperfections on the measured and predicted actuation stiffness, *Journal of the Mechanics and Physics of Solids* 53 (8) (2005) 1875–1891.

- 510 [12] J. W. Bird, M. J. Santer, J. F. Morrison, Adaptive Kagome Lattices for Near Wall Turbulence Suppression, in: 23rd AIAA/AHS Adaptive Structures Conference, no. 1, American Institute of Aeronautics and Astronautics, Reston, Virginia, 2015, pp. 1–20.
- [13] A. Leung, Actuation of kagome lattice structures, Proceedings of the 45th  
515 AIAA/ASME/ASCE/AHS/ASC Structures, Structural Dynamics & Materials Conference (2004) 19–22.
- [14] A. Leung, S. Guest, Single member actuation of kagome lattice structures, Journal of Mechanics of Materials and Structures 2 (2) (2007) 303–317.
- [15] S. Guest, On the determinacy of repetitive structures, Journal of the Me-  
520chanics and Physics of Solids 51 (3) (2003) 383–391.
- [16] G. R. Cowper, The Shear Coefficient in Timoshenko’s Beam Theory, Journal of Applied Mechanics 33 (2) (1966) 335.